Received February 24, 2021, accepted April 9, 2021, date of publication April 29, 2021, date of current version May 18, 2021.

Digital Object Identifier 10.1109/ACCESS.2021.3076701

Liquid-Solid Hybrid Memory Device Achieved by Unique Features of Ionic Liquids

HIROSHI SATO[1], HISASHI SHIMA[2], YUSEI HONMA[2], YASUHISA NAITOH[2], HIROYUKI AKINAGA[2], (Member, IEEE), TOSHIKI NOKAMI[3], TOSHIYUKI ITOH[3], AND KENTARO KINOSHITA[1]

[1]Department of Applied Physics, Tokyo University of Science, Katsushika, Tokyo 125-8585, Japan
[2]Device Technology Research Institute, National Institute of Advanced Industrial Science and Technology, Tsukuba 305-8565, Japan
[3]Center for Research on Green Sustainable Chemistry, Tottori University at Koyama, Tottori 680-8552, Japan

Corresponding author: Kentaro Kinoshita (kkinosita@rs.tus.ac.jp)

This work was supported in part by the Colors and Advanced Processing Department, NAGASE & Company Ltd.

ABSTRACT Ionic liquids (ILs), non-volatile liquids composed of cations and anions, have various attractive properties for electronic devices, such as wide potential windows. Combining ILs with electronic devices is presumed to be able to provide new options for realizing a sustainable internet of things society because such liquid-solid hybrid devices have the capability to act as a key in realizing further possibilities that cannot be achieved with all-solid-state devices. In this paper, we describe the development of IL-supplied conducting-bridge random access memory (IL-CBRAM) whose operating mechanism is the Cu filament formation/rupture caused by redox reactions in ILs as an electrochemical reaction field. Although the introduction of liquids into solid-state processes is challenging, we successfully demonstrated the reproducible memory operation of IL-CBRAM with a Cu/SiO_2/Pt structure and a microfabricated pore filled with IL in the SiO_2 layer. We also improved the wettability of the IL to SiO_2 by exposing it to Ar plasma, which was essential not only to obtain an IL thin film from the droplet but also to ensure pore filling by the IL before Cu deposition. The present device fabrication process for IL-CBRAM is highly reliable and compatible with conventional vacuum processes.

INDEX TERMS Artificial intelligence, Internet of Things, random access memory, vacuum technology.

I. INTRODUCTION

The driving force behind updates and improvements to electronic devices and their fabrication processes has always been in accordance with the needs of the time. As symbolized by the high-k gate dielectric materials in complementary metal-oxide-semiconductor (CMOS) devices [1] and Cu lines in large-scale integration (LSI) circuits [2], the introduction of emerging and functional materials into electronics has accelerated such technology updates. Although solid material was the primary component in past materials innovation in the field of electronics, the development of liquid materials is expected to generate a broader range of options for the development of new devices and processes required, particularly in order to fix the challenges present in an internet of things (IoT) society with tremendous energy consumption as a result of information processing. In this article, we propose a new technology that integrates ionic liquids (ILs) and solid-state memory elements. IL is a non-volatile liquid composed of cations and anions that have attractive properties for electronic devices, such as wide potential windows. Combining ILs with electronic devices is expected to provide new options for realizing a sustainable IoT society because such liquid-solid hybrid devices have the capability to act as a key in realizing further possibilities that cannot be achieved with all-solid-state devices. The introduction of new materials, such as ILs, has led to higher performance in numerous devices so far. ILs feature very good properties as reaction media in chemical reactions; they are less volatile, less flammable, have low toxicity and unique solubility in organic and inorganic materials [3]–[5] and are applicable to electronic devices, such as the gate insulator of field-effect transistors [6], [7]. Among these, IL is compatible with conducting-bridge random access memory (CBRAM) because it can be used as an electrochemical reaction field like electrochemical metal deposition [8]. CBRAM is a type

The associate editor coordinating the review of this manuscript and approving it for publication was M. Venkateshkumar.

This work is licensed under a Creative Commons Attribution 4.0 License. For more information, see https://creativecommons.org/licenses/by/4.0/

of nonvolatile memory with a high density, high speed and high-resistance ratio [9]–[12]. It has attracted interest as a next-generation nonvolatile memory due to its high performance and simple device architecture [13]–[21]. CBRAM has a simple cell structure in which an oxide layer is sandwiched between an electrochemically-active electrode (AE) that has a low standard electrode potential, e.g., comprising Cu and Ag, and an inactive electrode (IE) that has a high standard electrode potential, such as Pt and W. CBRAM could replace Flash and HDD to support the platforms of the IoT and other low-power applications [16], [17]. Also, I_{comp}-dependent-data-volatility enables unique applications in which I_{comp} is the value of the current below which a current is limited during set-switching. The nonvolatile nature of the data, stored by making the I_{comp} large, allows computers to achieve start-up instantly after being turned on, the so-called "instant-on" functionality. The volatile nature of data, stored by making the I_{comp} small, allows the manufacturing of neuromorphic devices [20]–[23]. We previously reported that the switching endurance and dispersion of operating voltages were improved by supplying IL to the polycrystalline metal oxide (poly-MO) layer of CBRAM with a Cu/poly-MO/Pt structure [24]–[28]. We established that the addition of a trace amount of an IL to the Cu/HfO_2/Pt cell as CBRAM effectively reduced the operating voltage and achieved an improved tolerance to external stimuli, such as voltage, temperature and pressure [29]. Among a variety of ILs, the addition of $Cu(Tf_2N)_2$ doped 1-butyl-3-methyl bis(trifluoromethylsulfonyl)amide ([bmim][Tf_2N]) was confirmed to significantly improve the cycling endurance [26]–[28]. For liquids other than ILs, supplying them affects the performance of CBRAM; the switching voltages of CBRAM decrease when increasing the polarity of supplied liquids [29]. However, these experiments were performed using a test structure that showed low affinity with solid-state processes and could not be of practical use; a drop of liquid was supplied to the surface of poly-MO film prepared on a Pt-IE and then a Cu probe was brought into contact with the surface through the droplet of the liquid, constituting a Cu probe/poly-MO/Pt structure. To increase the affinity with solid-state processes a liquid supply must be incorporated during the vacuum processes. Above all, the introduction of liquids into solid-state processes is challenging, although it is necessary to discover further possibilities that cannot be achieved with all-solid-state devices.

In this study, we successfully demonstrated the fabrication of a solid-liquid hybrid device confining IL in the sandwiched structure of Cu/SiO_2/Pt, in which a single pore was artificially formed in the SiO_2 layer. This was achieved due to the finding that the exposure to Ar plasma increases the wettability of IL, in addition to the non-volatility inherent in IL. The former enhances capillary condensation of IL into the pore and the latter enabled IL to be introduced into the vacuum process of sputtering. We demonstrated the memory operation of an IL-supplied CBRAM device containing an artificially-formed single pore filled with IL (IL-CBRAM). We confirmed that a 0.4 M, mol/L, Cu-doped IL-CBRAM exhibited a short switching time (<1.0 μs) with a low voltage (<3.0 V) and low switching voltage dispersion (<0.6 V).

II. UNIQUE FEATURES OF ILS IMPORTANT FOR PORE FILLING

We prepared IL-CBRAM devices with a stack structure of Cu/SiO_2/Pt/Ta/SiO_2 substrate (Cu/SiO_2/Pt) that contained an artificially-formed pore filled with IL in the SiO_2 layer, as is shown in Figure 1. The diameter of the pore was 1 μm and the 1-nm-thick Ta layer was inserted between the SiO_2 and Pt-IE layers as an adhesion layer. A small amount of IL was dropped on the SiO_2 substrate approximately at the position where the pore exists, and then the Cu-AE was formed using the sputtering method. During sputtering, the IL is exposed to Ar plasma. Figures 2(a), (b) and (c) show the optical microscope images of the IL on the substrate before exposure to Ar plasma, immediately after exposure, and 3 sec after exposure, respectively. Figures 2(d), (e) and (f) show the cross-sectional drawings of the pore corresponding to Figures 2(a), (b) and (c), respectively. The area where IL was spread is indicated by the dotted line. Before plasma exposure, IL was clustered as a droplet, as shown in Figures 2(a) and (d), suggesting poor wettability against an SiO_2 surface. It was difficult to form an electrode on the droplet-shaped IL. Furthermore, because the radius of the pore was small, the supplied IL droplet may be located outside of the pore, as shown in Figure 2(d). However, this problem can be solved by exposure to Ar plasma. IL began to disperse when the substrate was exposed to Ar plasma in a vacuum before Cu deposition (Figures 2(b) and (e)). After 3 sec of exposure, the IL expanded to 10 times the area it had before exposure (Figures 2(c) and (f)). Although reports exist on the improvement of IL's wettability due to surface modification from using a silane coupling agent [30], the results shown in Figure 2 may be due to the modification of the SiO_2 surface. In general, hydroxy groups of -OH are adsorbed on the surface of SiO_2 and form a silanol group of Si-OH, which yields the high-polarity of the SiO_2 surface [31]. The polar organic molecules were easily hydrogen-bonded to this polar surface. Then, non-polar organic molecules were further bonded on the polar organic molecules by van der Waals force. Before Ar plasma exposure, the high-polarity of the SiO_2 surface was compensated by those molecules. The exposure to Ar plasma broke the weak bonds of the hydrogen- and van der Waals-bonds and only the strong bond of Si-OH

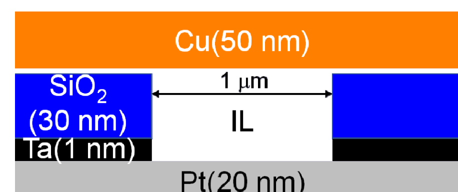

FIGURE 1. The schematic of the IL-CBRAM.

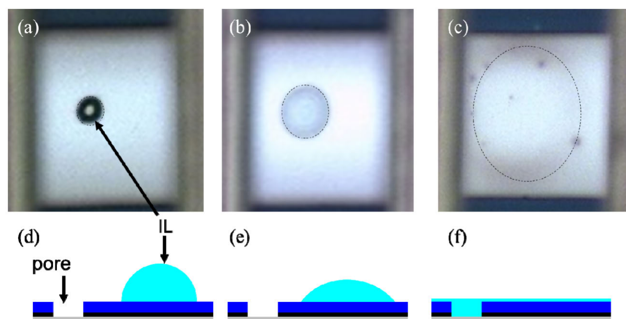

FIGURE 2. Optical microscope images and cross-sectional schematic of IL (a), (d) before the exposure to Ar plasma, (b), (e) immediately after the exposure and (c), (f) 3 sec after starting the exposure.

remained; as a result, the polar surface was exposed. Because the wettability of the polar liquid, including the IL, became high for the polar surface, the wettability of the IL was improved by Ar plasma exposure.

III. DEVICE FABRICATION

A. FABRICATION PROCESS OF THE STACK STRUCTURE

We fabricated an IL-CBRAM device with a stack structure comprising a Cu/SiO_2/Pt/Ta/SiO_2 substrate by using the following procedure: (i) Ta (1 nm), Pt (20 nm) and Ta (1 nm) layers were sequentially formed on an SiO_2 wafer, which worked as an IE, *via* a magnetron sputtering method; (ii) a 30-nm-thick SiO_2 layer was formed through chemical vapor deposition; (iii) a pore with a 1 μm diameter was formed through photolithography and the milling of the SiO_2 layer and upper Ta layer (the optical microscope image of the pore and its enlarged view with SEM are shown in Figures 3(a) and (b), respectively); (iv) IL was provided on the SiO_2 surface at which a cross-point between the Cu-AE and Pt-IE ultimately formed (we provided a few μl of IL adhered to the tip of a probe, due to the surface tension on each pore, as is shown in Figure 3(c)) and (v) a 50-nm-thick Cu-AE was sputtered using the magnetron sputtering method. During sputtering, the SiO_2 surface's wettability to the IL was drastically enhanced due to plasma exposure; thus, the IL spread uniformly over the surface of the SiO_2 layer and permeated the pore as well. Figure 3(d) shows an optical microscopic image of our device. The stack structure was located at the cross-point of the AE and IE. Despite being sputtered on the IL, the AE took a flat form, with no IL leaks to the outside of the cross-point of the electrodes, as shown in the enlarged view of the cross-point with SEM in Figure 3(e). For an IL, we selected Cu-doped 1-butyl-3-methylimidazolium bis (trifluoromethylsulfonyl)amide ([bmim][Tf_2N]) [25], which is the 0.4 M solution of Cu(II) bis(trifluoromethylsulfonyl) amide (Cu[Tf_2N]$_2$) in [bmim][Tf_2N], because the switching endurance and dispersion of the operating voltages were confirmed to be improved in previous studies [24]–[26]. The [bmim][Tf_2N] in which 0.4 M Cu[Tf_2N]$_2$ is dissolved is simply termed IL, hereafter, since this is the only IL used in this study. A voltage was applied to the Cu-AE with the Pt-IE grounded. Subsequently, XPS measurements were

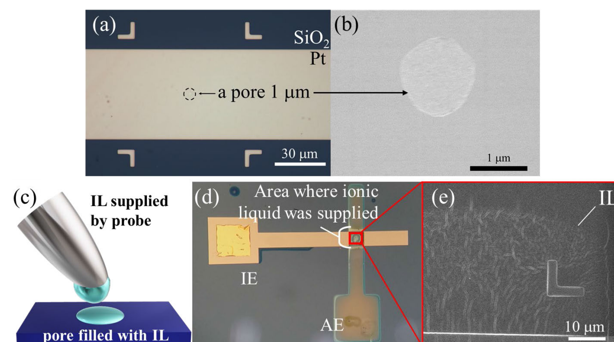

FIGURE 3. (a) The optical microscope image of IL-CBRAM before sputtering AE; (b) the SEM image of a pore with a diameter of 1 μm was fabricated in the memory layer before sputtering AE; (c) supplying IL to the pore before sputtering AE; (d) optical microscope image of the IL-CBRAM after AE sputtering; (e) enlarged view of the crosspoint in (d) with SEM after AE sputtering.

conducted using ULVAC-PHI Quantera II which employs a monochromated Al Ka X-ray source (1486.6 eV). The photoelectron take-off angle in the present XPS measurement was 45°. We measured current voltage (I–V) characteristics using a semiconductor parameter analyzer (Agilent B1500A). For the voltage sweep measurements, we fixed the current compliance value (I_{comp}) at 200 μA for the set process to limit the current flow. For the pulse measurement, we inserted a junction transistor in series with an IL-CBRAM device to limit the excessive growth of the filaments.

B. FABRICATION PROCESS OF THE SLIT STRUCTURE

We fabricated devices with a slit structure to observe how filaments form and rupture in the IL-filled pore. Figure 4(a) presents the schematic of the slit structure, which was formed by milling both the upper Ta and the SiO_2 layers of the IL-CBRAM, using the Cu-AE as a hard mask, so that the inside of the pore could be observed. Figure 4(b) shows an AFM image of the slit structure. The bright contrast regions in the AFM image correspond to a high position and the dark contrast regions to a low one. Figure 4(a) is a schematic diagram within the red dotted line in Figure 4(b). Figure 4(c) shows unevenness along the line A-B in Figure 4(b), which crosses the slit area. The slit had a width of 80 nm and a depth of 30 nm. During the measurement of the I–V characteristics, we added IL to the structure and then washed it out with ethanol before observing it with an SEM.

C. CHEMICAL STATE OF CU FILM FORMED ON IL

We also evaluated the chemical state of Cu sputtered on IL in order to confirm the existence of the metallic Cu state as AE by conducting the micro XPS measurement. The XPS measurement for IL was carried out using an IL drop on the SiO_2/Si substrate. The analyzed area for IL is around 100 μm in diameter. On the other hands, the specimens of Cu (10 nm)/IL and Cu (50 nm)/IL for the XPS measurements were prepared by the same procedure as the IL-CBRAM device as shown in Figure 5(a) and (b), respectively. The analyzed area for these sample is around 20 μm in diameter, which is located on the inside of the red circles in those

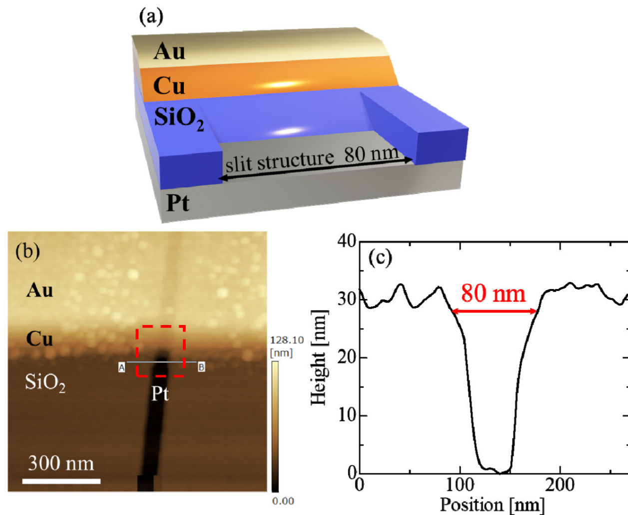

FIGURE 4. (a) A schematic of the slit structure, which is in a situation similar to that in the pore and enables in-situ observation; (b) AFM image of the slit structure; (c) AFM profiles along the line A-B in Figure 4(b) crossing the slit area.

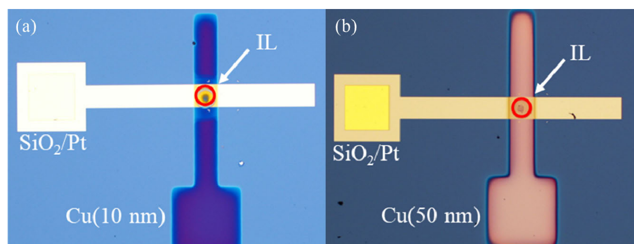

FIGURE 5. The photograph of (a) Cu(10 nm)/IL and (b) Cu(50 nm)/IL. The analyzed area (~ 20 μm in diameter) is inside the red circles.

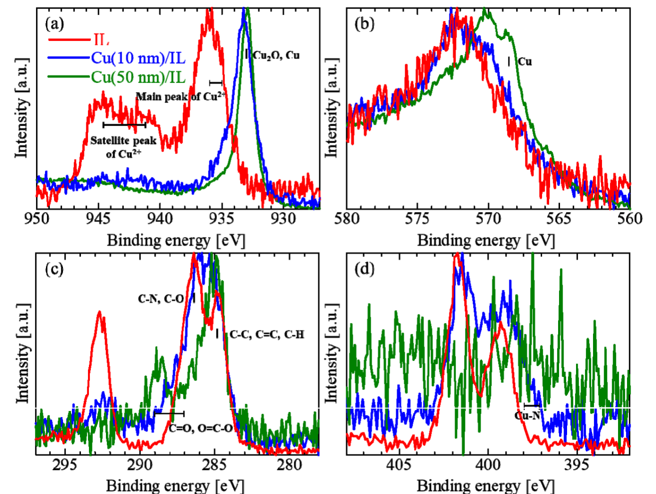

FIGURE 6. (a) Cu $2p_{3/2}$, (b) Cu LMM, (c) C1s and (d) N1s spectra for IL (red), Cu (10 nm)/IL (blue), and Cu (50 nm)/IL (green).

figures. Figures 6(a) shows the Cu $2p_{3/2}$ XPS spectrum. Because the marked satellite peak in Cu $2p_{3/2}$ XPS spectra shown in Figure 6(a) is generally typical of the Cu divalent ions (Cu^{2+}) state, Cu in the preset IL is thought to be in the Cu^{2+} state. The main peak in Cu $2p_{3/2}$ XPS spectrum for IL located at the binding energy (B.E.) of around 935 eV was also reported in the XPS spectra for [bmim][Tf_2N]:Cu(Tf_2N)$_2$ (1:1) containing a highly concentrated solution of Cu^{2+} ions [32]. After sputtering the Cu thin film on IL, the main peak position in the Cu $2p_{3/2}$ XPS spectra in Cu (10 nm)/IL and Cu (50 nm)/IL shifted toward the lower B.E. of around 933 eV. According to the previous reports, the possible candidate for the peak at this B.E. is Cu_2O (932.4 eV) and/or Cu (932.6 eV) [33]. Although it is difficult to distinguish between Cu_2O and Cu from the Cu $2p_{3/2}$ XPS spectrum, they are distinguishable by investigating the Cu LMM auger spectrum as shown in Figure 6(b). The auger signal derived from the metallic Cu is observed at the lower B.E. (higher kinetic energy) compared to Cu_2O, which was previously confirmed in Cu_2O reduced in H_2 at the elevated temperature [33]. Therefore, the auger signal in the B.E. range roughly from 568 to 569 eV observed in Cu (50 nm)/IL can be attributed to the metallic Cu. Shown in Figures 6(c) and (d) are the C1s and N1s XPS spectra, respectively. In the C1s XPS spectra for both IL and Cu (10 nm)/IL, the C1s signals originated from [Tf_2N] (B.E.: 292∼294 eV) and [bmim] (B.E.: 283∼288 eV) are observed [34], while such characteristics disappear in Cu(50 nm)/IL. In analogy with the C1s XPS spectra, two peaks in the N1s spectrum characterizing [bmim][Tf_2N], i.e. one peak at lower B.E. derived from the imidazolium ring and the other peak at higher B.E. related to the anion, are clearly observed for IL and Cu (10 nm)/IL. On the other hands, the intensity for the N1s signal in Cu (50 nm)/IL was below the detection limit. Since the detection depth in the present XPS measurement is 4∼5 nm, the C1s and N1s signals observed in Cu (10 nm)/IL indicate that the thickness of the Cu film on IL is thinner than 10 nm. In addition to that, it should be noted that the N1 signal assigned to the bonding between Cu and N (B.E.: 396∼397 eV) is the highest in Cu (10 nm)/IL [35]. The possible scenario for the metallic Cu thin film formation on IL deduced from the XPS spectra is as following. At the beginning of the Cu sputtering process, the reactive layer between Cu and [Tf_2N] is formed on the surface of IL, although a part of the sputtered Cu submerges in IL. When the amount of the metallic Cu is insufficient, all of the Cu layer is oxidized into Cu_2O after Cu (10 nm)/IL is taken out from the vacuum chamber. With increasing the thickness of the Cu layer, the metallic Cu can remain under the surface oxide film in Cu (50 nm)/IL.

D. FORMATION OF INSULATING FILM BY FILLING PORE WITH IL

Figure 7 shows I–V characteristics of the IL-CBRAM and Control in the initial state. Here, the Control was a device in which Cu was deposited on the AE without supplying IL to the pore prepared by the same process as IL-CBRAM. The insets show the cross-sectional schematic of the pore for the Control (right) and IL-CBRAM (left). When the IL was not supplied in the pore, the device was initially conductive due to the deposition of Cu in the pore as shown in

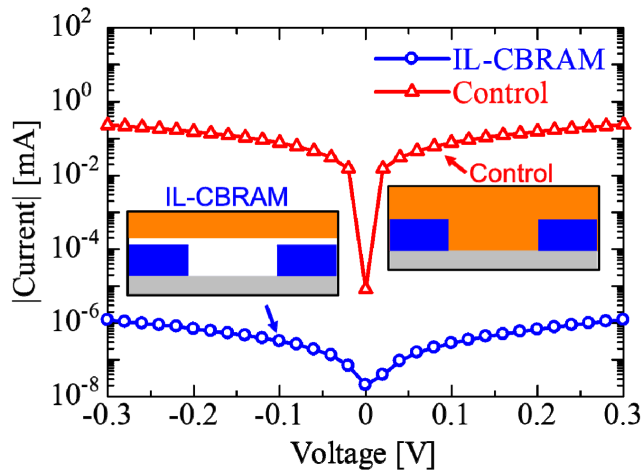

FIGURE 7. ***I–V*** **characteristics of IL-CBRAM and Control in the initial state. Insert: cross-sectional schematic of the pore for Control (right) and IL-CBRAM (left).**

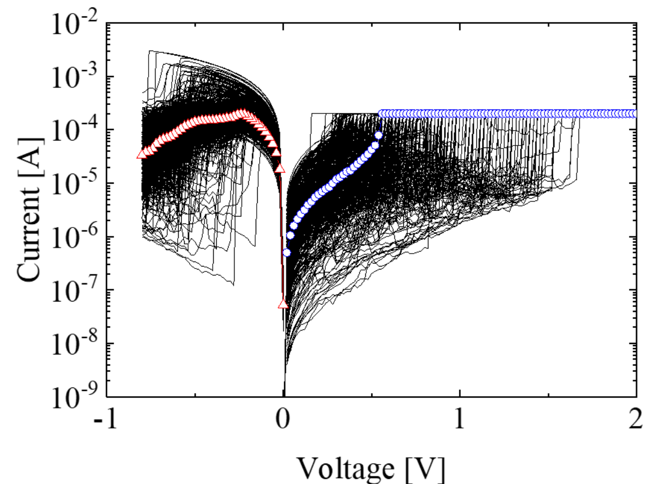

FIGURE 8. ***I–V*** **characteristics of the IL-CBRAM. The black lines show** ***I–V*** **characteristics for continuously repeated 500 cycles. The blue circles and red triangles represent the median values of the** ***I–V*** **data for set and reset cycles, respectively.**

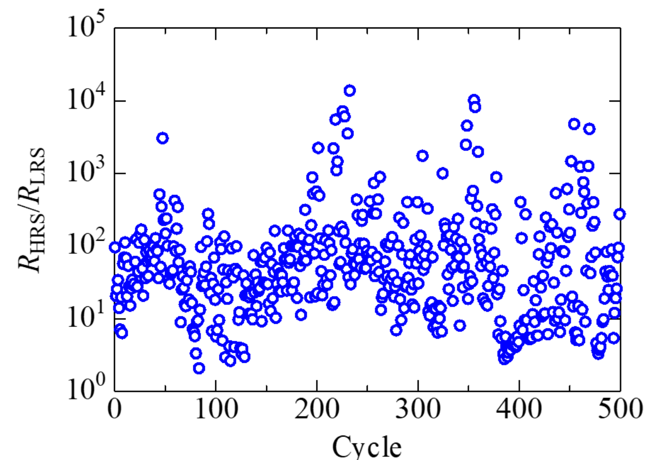

FIGURE 9. **The values of** R_{HRS}/R_{LRS} **for 500 cycles of IL-CBRAM.**

the cross-sectional schematic of the Control. However, IL-CBRAM had a much higher resistance than the Control had, indicating that IL-CBRAM was insulated in its initial state. This suggested that IL-CBRAM was supplied with the IL in the pore and Cu film was formed on the pore as shown in the cross-schematic of the pore for IL-CBRAM. Surprisingly, the electrodes sputtered onto the plasma-exposed IL were stable. At this time, we have supplied IL using probes, but we are considering supplying IL with an inkjet for practical purposes.

IV. EVALUATION OF ELECTRICAL CHARACTERISTICS

A. VOLTAGE SWEEP MEASUREMENT

By applying a positive bias to the AE, metal ions were positively ionized and eluted from the AE. Eluted metal ions diffused into the oxide layer, forming Cu filaments that connected the AE and IE and resulted in a low-resistance state (LRS). Subsequently, by applying a negative bias to the AE, the filaments were ruptured, returning device to a high-resistance state (HRS). The switching from HRS to LRS, and vice versa, is called 'set' and 'reset', respectively. The HRS and LRS were both stably retained; set and reset can be caused by applying negative and positive biases, respectively. Hence, this device worked as nonvolatile memory. Figure 8 displays the I–V characteristics of IL-CBRAM, with 500 cycles. The blue circles and red triangles indicate the median values for the set and reset processes, respectively, of the 500 I–V cycles represented by the solid lines. We observed bipolar resistive switching between a set and a reset, with the application of positive and negative bias voltages respectively, which suggested that IL-CBRAM works based on the same operating mechanism as the conventional CBRAM. Figure 9 shows the value of R_{HRS}/R_{LRS} for 500 cycles of IL-CBRAM. This had an on-off ratio of 2.04 $\times$ 10^0–1.36 $\times$ 10^5, which allowed for 500 cycles of stable operation. Figure 10(a) shows the cumulative probabilities of V_{set} and V_{reset} for IL-CBRAM. Table 1 summarizes the average and relative standard deviation (RSD) of the V_{set}, V_{reset}, R_{HRS}, and R_{LRS} for IL-CBRAM. The average value and RSD of the V_{set} were 0.65 V and 0.48, respectively. On the other hand, the average value and RSD of V_{reset} were 0.34 V and 0.40, respectively. According to Ref. 29, the DC voltage application exceeding 3 V results in the decomposition of IL [29]. However, since the absolute values of both V_{set} and V_{reset} in Fig. 10(a) are sufficiently smaller than 3 V even in consideration of the errors, the resistance switching is possible without causing decomposition of IL in the present IL-CBRAM. Therefore, the nonvolatility and electrochemical stability of IL are ensured under the measurement conditions in this study.

Figure 10(b) shows R_{HRS} and R_{LRS} for IL-CBRAM. The average value and RSD of R_{HRS} were 1.8 $\times$ $10^5\Omega$ and 3.2, respectively, and the respective average value and RSD of R_{LRS} were 1.1 $\times$ 10^3 Ω and 0.50, respectively. The operating voltages (V_{set} and V_{reset}) of the IL-CBRAM are supposed to be influenced by the impurity in IL such as water

TABLE 1. The average and RSD of the V_{SET}, V_{RESET}, R_{HRS}, and R_{LRS} for IL-CBRAM.

	V_{SET}	V_{RESET}	R_{HRS}	R_{LRS}
Average	0.65 V	0.34 V	$1.8\times10^5\,\Omega$	$1.1\times10^3\,\Omega$
RSD	0.48	0.40	3.2	0.50

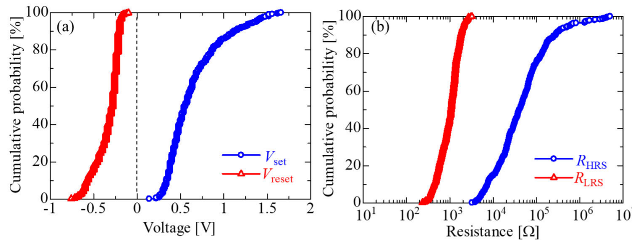

FIGURE 10. (a) Cumulative probabilities of V_{set} and V_{reset} for IL-CBRAM; (b) cumulative probabilities of R_{HRS} and R_{LRS} for IL-CBRAM.

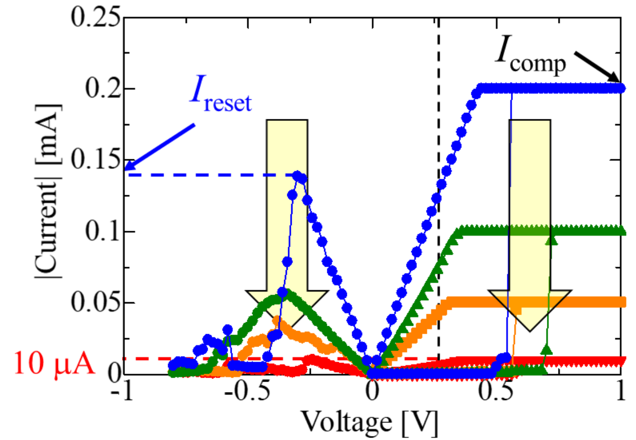

FIGURE 11. I–V characteristics of IL-CBRAM under different I_{comp} of 200, 100, 50 and 10 μA.

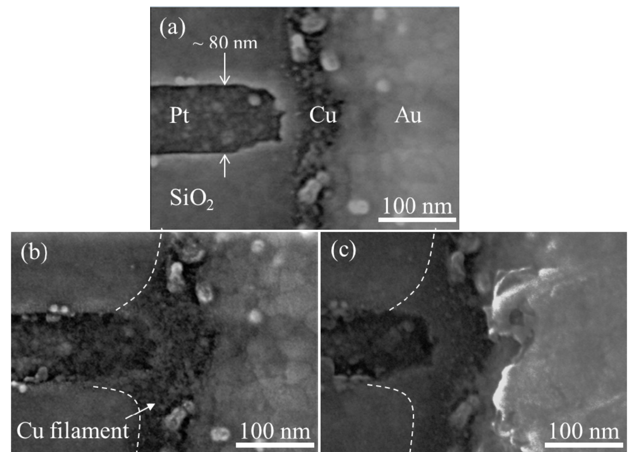

FIGURE 12. FE-SEM images of the slit-type Cu/IL/Pt device observed: (a) in the initial state; (b) after set and (c) after reset processes. As the contrast changes inside the dotted line, the formation and rupture of the filament can be confirmed.

molecules [26]. Because the present device fabrication process includes the IL supply in the air, the water content in IL is thought to vary during this IL supply process as a result of the moisture absorption. The variability of the water content in IL may result in the lot-to-lot variation of the operating voltages, and also leads the variation in resistances (R_{HRS} and R_{LRS}). The development of the IL supply process in vacuum may be required to stabilize the water content in IL, which is expected to increase the reliability of the device fabrication process for the IL-CBRAM.

Then, we investigated the relationship between I_{comp} and reset current (I_{reset}), where the maximum current during the reset process was defined as I_{reset}. Reducing the I_{reset} was necessary to achieve the low-power operation of resistive switching memories. Figure 11 shows the I–V curves for I_{comp} = 10, 50, 100 and 200 μA. Note that a reduced I_{comp} led to a corresponding decrease in I_{reset}, thus maintaining the relationship $I_{reset} \leq I_{comp}$ to lower than 10 μA, meaning that I_{reset} can be controlled by I_{comp}. We observed the deterioration of data retention for a lower I_{comp} value. In particular, the data retention time for the I_{comp} of 10 μA was less than 1 min. The high controllability of I_{reset} by I_{comp} to the small values lower than 10 μA was consistent with what has been observed in conventional CBRAM, suggesting similar memory characteristics of IL-CBRAM to conventional CBRAM [36]–[38].

B. DIRECT OBSERVATION OF FILAMENT FORMATION IN THE PORE USING SLIT STRUCTURES

We observed how filaments form and rupture in the IL-filled pore. Field emission scanning electron microscope (FE-SEM) images of the slit structure in the initial state, after set, and after reset, respectively, are shown in Figures 12(a), (b) and (c). The width of the slit section in the present device was 80 nm, which was in agreement with the width of the slit estimated by the aforementioned AFM image. In the initial state, the SiO_2 layer could be observed between the Cu layer and Pt-IE layer. After set-switching, a Cu filament consisting of thin Cu fibers extended to the IE from the Cu-AE, as depicted in the dotted line in Figure 12(b). The Cu filament connected the Cu-AE and Pt-IE, lowering the resistance. These results indicated that the electrochemically-dissolved Cu ions migrated to the Pt-IE layer, moving in IL rather than in bulk SiO_2 to form a filament because they were more easily diffused in the IL. In addition, the filament shape differed from the dendrite structure in the planar devices [39]. Moreover, the same device was reset to a HRS. The dotted line in Figure 12(c) indicates the area where the Cu filament was present prior to reset switching. Again, the Cu filament disappeared in the Cu-AE layer, with the SiO_2 layer being visible. This indicates that the formation and rupture of the Cu filament, that is, the set and reset, are both reproducible and repeatable. To the best of our knowledge, this is the first direct observation of the formation of a Cu filament and its rupture in IL-CBRAM.

C. PULSE MEASUREMENT

Figure 13 shows the measurement results and how we evaluated the set speed (t_{set}), with Figures 13(a) and (b) showing, respectively, the height of the applied voltage pulse and resistance after the pulse injection. At the pulse count of 1 (#1), we applied a −2.0 V high-voltage pulse to IL-CBRAM and reset the resistance to a HRS, where the pulse width (t'_w) was fixed at 10^{-5} s. Next, at pulse #2–51, we applied voltage pulses from 0–5.0 V in increments of 0.1 V, as is shown in Figure 13(a). Here, the pulse width (t_w) was fixed at 10^{-6} s. We observed a variation in resistance from high to low at pulse #20, as shown in Figure 13(b), which shows that set-switching occurred at a pulse height of 1.9 V for the t_w of 10^{-6} s. Repeating these series of measurements, we obtained the necessary set of pulse heights required to set IL-CBRAM and discuss them statistically. We performed the same measurement for the reset processes. Accordingly, Figure 13(c) shows the pulse heights required to set and reset the 0.4-M Cu-doped IL-CBRAM, i.e., V_{set} and V_{reset}, for the pulse measurement for various $t_{w.}$ The value of t_{set} and the reset speed (t_{reset}) was 10^{-6} s for the V_{set} of 1.9 V and 10^{-7} s for the V_{reset} of 1.5 V. Because a transistor was connected during the set to limit the excessive growth of filaments, the parasitic capacitance and channel resistance of the transistor allowed us to use a pulse width $\leq 10^{-6}$ s. The transistor was removed when measuring the t_{reset}. In particular, the value of t_{reset} was more than two orders of magnitude shorter than t_{set} when compared with the same absolute values of V_{set} and V_{reset}. For example, the green arrow in the figure indicates that with a switching voltage of 1.0 V, t_{reset} would be approximately three orders of magnitude shorter than t_{set}. Such a slower set process was attributable to the intrinsic nature of IL, which consists of different anions and cations, not polar molecules. Cations of the IL form the inner Helmholtz layer covering the cathode's surface, and the positively charged Cu ions were prevented from accessing the cathode, causing the increase in V_{set} [27] and making t_{set} longer. Our idea to overcome this issue was to use Cu doped solvate ionic liquid of Triglyme (G3)-$Cu(TF_2N)_2$ [27] instead of Cu ion-doped IL. G3 is an electrically-neutral chainlike molecule that weakly coordinates with Cu ions. We postulated that the Cu filament would be smoothly produced on the electrode's surface with the help of coordination from G3 while avoiding the segregation of Cu ions. In this way, the theoretical expectation of electrochemical diffusion in liquid electrolytes is simpler than in solid electrolytes. Therefore, IL-CBRAM can more directly correlate the electrochemical parameters of metals in ILs with the memory operating performances, enabling us to control them through the high design ability of ILs. Several papers exist on the resistive switching device in which IL is used as the resistive switching matrix [40]–[42]. In all aspects, the device size, switching voltage, switching speed and fabrication process led to the reasonable assertion that the present device had the highest degree of affinity for conventional CMOS technology. Toward the statistical evaluation of the device-to-device operating performance distributions using large number of IL-CBRAMs, the higher mass productivity is required for the method of supplying ILs. The development of the spin-coating or inkjet technology for ILs will bridge the gap between the present fabrication process and large-scale production.

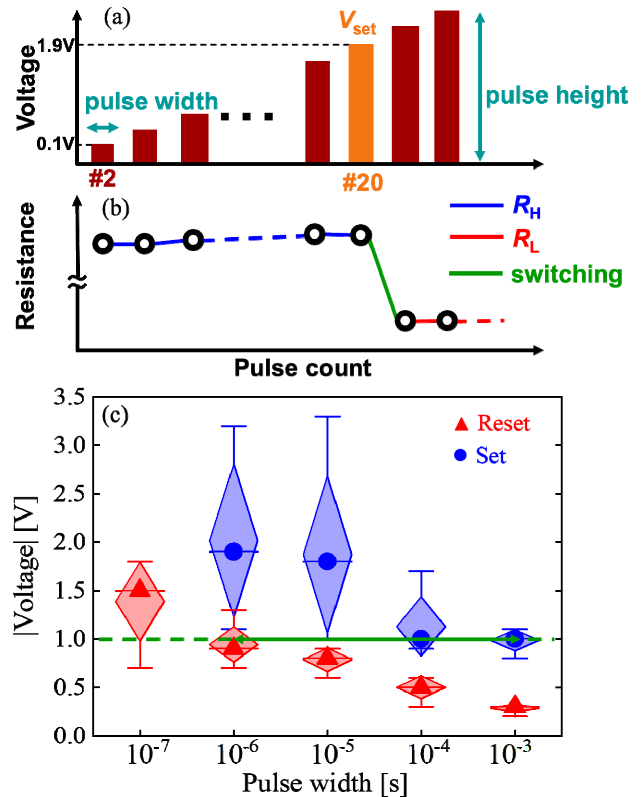

FIGURE 13. (a) Height of the applied voltage pulse; (b) resistance after the pulse injection and (c) pulse heights vs. pulse width required to set and reset IL-CBRAM. After reset (#1, which is not shown), as is shown in (a), the voltage pulses were sequentially injected while increasing the pulse height by 0.1 V each. The resistive switching time of IL-CBRAM was less than 10^{-6} s.

V. CONCLUSION

The nonvolatility of the IL enabled us to use it in a vacuum process, and we were able to fabricate a memory device with a $Cu/SiO_2/Pt$ structure that has a microfabricated pore filled with IL in its SiO_2 layer. A key finding for the fabrication of this new memory device, called IL-CBRAM, was that wettability of IL with respect to the SiO_2 surface was enhanced by Ar plasma exposure to SiO_2. This was essential to ensure pore filling by IL before Cu deposition and to obtain an IL thin film from the droplet, enabling the following Cu electrode deposition onto it. We successfully demonstrated the reproducible memory operation, although the introduction of liquids into solid-state processes was challenging. In addition, the use of IL-CBRAM with a slit structure provided us with an insight into the switching mechanism: IL provides a good electrochemical reaction field where Cu filament formation/rupture is caused by redox reactions. The presented device fabrication process is highly reliable and compatible with conventional vacuum processes, shedding light on the creation of emerging

liquid-solid hybrid devices that will support the technology of the coming era.

ACKNOWLEDGMENT

The authors thank Enago (www.enago.jp) for the English language review.

REFERENCES

[1] D. Edelstein, J. Heidenreich, R. Goldblatt, W. Cote, C. Uzoh, N. Lustig, P. Roper, T. McDevitt, W. Motsiff, A. Simon, J. Dukovic, R. Wachnik, H. Rathore, R. Schulz, L. Su, S. Luce, and J. Slattery, "Full copper wiring in a sub-0.25 μm CMOS ULSI technology," in *IEDM Tech. Dig.*, Dec. 1997, pp. 773–776.

[2] G. D. Wilk and R. M. Wallace, "Electrical properties of hafnium silicate gate dielectrics deposited directly on silicon," *Appl. Phys. Lett.*, vol. 74, no. 19, pp. 2854–2856, May 1999.

[3] P. Wasserscheid and T. Welton, *Ionic Liquids in Synthesis*. Hoboken, NJ, USA: Wiley, 2002, p. 1.

[4] J. P. Hallett and T. Welton, "Room-temperature ionic liquids: Solvents for synthesis and catalysis. 2," *Chem. Rev.*, vol. 111, no. 5, pp. 3508–3576, May 2011.

[5] A. Berrueta, A. Ursua, I. S. Martin, A. Eftekhari, and P. Sanchis, "Supercapacitors: Electrical characteristics, modeling, applications, and future trends," *IEEE Access*, vol. 7, pp. 50869–50896, 2019.

[6] Y. Saito and Y. Iwasa, "Ambipolar insulator-to-metal transition in black phosphorus by ionic-liquid gating," *ACS Nano*, vol. 9, no. 3, pp. 3192–3198, Mar. 2015.

[7] S. Ono, S. Seki, R. Hirahara, Y. Tominari, and J. Takeya, "High-mobility, low-power, and fast-switching organic field-effect transistors with ionic liquids," *Appl. Phys. Lett.*, vol. 92, pp. 103313-1–103313-3, Mar. 2008.

[8] S. Arimoto, H. Kageyama, T. Torimoto, and S. Kuwabata, "Development of *in situ* scanning electron microscope system for real time observation of metal deposition from ionic liquid," *Electrochem. Commun.*, vol. 10, no. 12, pp. 1901–1904, Dec. 2008.

[9] R. Waser, R. Dittmann, G. Staikov, and K. Szot, "Redox-based resistive switching memories–nanoionic mechanisms, prospects, and challenges," *Adv. Mater.*, vol. 21, nos. 25–26, pp. 2632–2663, Jul. 2009.

[10] W. Banerjee, "Challenges and applications of emerging nonvolatile memory devices," *Electronics*, vol. 9, no. 6, p. 1029, Jun. 2020.

[11] Y. Deng, P. Huang, B. Chen, X. Yang, B. Gao, J. Wang, L. Zeng, G. Du, J. Kang, and X. Liu, "RRAM crossbar array with cell selection device: A device and circuit interaction study," *IEEE Trans. Electron Devices*, vol. 60, no. 2, pp. 719–726, Feb. 2013.

[12] R. Waser, D. Ielmini, H. Akinaga, H. Shima, H.-S. P. Wong, J. J. Yang, and S. Yu, *Introduction to Nanoionic Elements for Information Technology, Resistive Switching: From Fundamentals of Nanoionic Redox Processes to Memristive Device Applications*. New York, NY, USA: Wiley, 2016, pp. 1–29.

[13] S. Ginnaram, J. T. Qiu, and S. Maikap, "Role of the Hf/Si interfacial layer on the high performance of MoS_2-based conductive bridge RAM for artificial synapse application," *IEEE Electron Device Lett.*, vol. 41, no. 5, pp. 709–712, May 2020.

[14] T. Hasegawa, Y. Itoh, H. Tanaka, T. Hino, T. Tsuruoka, K. Terabe, H. Miyazaki, K. Tsukagoshi, T. Ogawa, S. Yamaguchi, and M. Aono, "Volatile/nonvolatile dual-functional atom transistor," *Appl. Phys. Exp.*, vol. 4, no. 1, Jan. 2011, Art. no. 015204.

[15] S. Muto, R. Yonesaka, A. Tsurumaki-Fukuchi, M. Arita, and Y. Takahashi, "Observation of conductive filament in CBRAM at switching moment," *ECS Trans.*, vol. 80, no. 10, pp. 895–902, Oct. 2017.

[16] Z. Dong, H. Zhao, D. DiMarzio, M.-G. Han, L. Zhang, J. Tice, H. Wang, and J. Guo, "Atomically thin CBRAM enabled by 2-D materials: Scaling behaviors and performance limits," *IEEE Trans. Electron Devices*, vol. 65, no. 10, pp. 4160–4166, Oct. 2018.

[17] J. R. Jamenson, P. Blanchard, J. Dinh, N. Gonzales, V. Gopalakrishnan, B. Guichet, S. Hollmer, S. Hsu, G. Intrater, D. Kamalanathan, and D. Kim, "Conductive bridging RAM (CBRAM): Then, now, and tomorrow," *ECS Trans.*, vol. 75, pp. 41–54, Aug. 2016.

[18] M. Lübben, S. Menzel, S. G. Park, M. Yang, R. Waser, and I. Valov, "SET kinetics of electrochemical metallization cells: Influence of counter-electrodes in SiO_2/Ag based systems," *Nanotechnology*, vol. 28, no. 13, Mar. 2017, Art. no. 135205.

[19] M. Suri, D. Querlioz, O. Bichler, G. Palma, E. Vianello, D. Vuillaume, C. Gamrat, and B. DeSalvo, "Bio-inspired stochastic computing using binary CBRAM synapses," *IEEE Trans. Electron Devices*, vol. 60, no. 7, pp. 2402–2409, Jul. 2013.

[20] J.-H. Ryu, B. Kim, F. Hussain, M. Ismail, C. Mahata, T. Oh, M. Imran, K. K. Min, T.-H. Kim, B.-D. Yang, S. Cho, B.-G. Park, Y. Kim, and S. Kim, "Zinc tin oxide synaptic device for neuromorphic engineering," *IEEE Access*, vol. 8, pp. 130678–130686, 2020.

[21] J.-H. Cha, S. Y. Yang, J. Oh, S. Choi, S. Park, B. C. Jang, W. Ahn, and S.-Y. Choi, "Conductive-bridging random-access memories for emerging neuromorphic computing," *Nanoscale*, vol. 12, no. 27, pp. 14339–14368, 2020.

[22] K. Moon, S. Lim, J. Park, C. Sung, S. Oh, J. Woo, J. Lee, and H. Hwang, "RRAM-based synapse devices for neuromorphic systems," *Faraday Discuss.*, vol. 213, pp. 421–451, Feb. 2019.

[23] Q. Wan, M. T. Sharbati, J. R. Erickson, Y. Du, and F. Xiong, "Emerging artificial synaptic devices for neuromorphic computing," *Adv. Mater. Technol.*, vol. 4, no. 4, Apr. 2019, Art. no. 1900037.

[24] A. Harada, H. Yamaoka, S. Tojo, K. Watanabe, A. Sakaguchi, K. Kinoshita, S. Kishida, Y. Fukaya, K. Matsumoto, R. Hagiwara, H. Sakaguchi, T. Nokami, and T. Itoh, "Improved performance of a conducting-bridge random access memory using ionic liquids," *J. Mater. Chem. C*, vol. 4, no. 30, pp. 7215–7222, 2016.

[25] A. Harada, H. Yamaoka, K. Watanabe, K. Kinoshita, S. Kishida, Y. Fukaya, T. Nokami, and T. Itoh, "Copper ion-containing ionic liquids provide improved endurance and switching voltage distributions of conducting-bridge random access memory," *Chem. Lett.*, vol. 44, no. 11, pp. 1578–1580, Nov. 2015.

[26] A. Harada, H. Yamaoka, R. Ogata, K. Watanabe, K. Kinoshita, S. Kishida, T. Nokami, and T. Itoh, "Enhanced stability of the HfO_2 electrolyte and reduced working voltage of a CB-RAM by an ionic liquid," *J. Mater. Chem. C*, vol. 3, no. 27, pp. 6966–6969, 2015.

[27] H. Yamaoka, T. Yamashita, A. Harada, A. Sakaguchi, K. Kinoshita, S. Kishida, S. Hayase, T. Nokami, and T. Itoh, "Significantly improved performance of a conducting-bridge random access memory (CB-RAM) device using copper-containing glyme salt," *Chem. Lett.*, vol. 46, no. 12, pp. 1832–1835, Dec. 2017.

[28] K. Kinoshita, A. Sakaguchi, A. Harada, H. Yamaoka, S. Kishida, Y. Fukaya, T. Nokami, and T. Itoh, "Improvement of switching endurance of conducting-bridge random access memory by addition of metal-ion-containing ionic liquid," *Jpn. J. Appl. Phys.*, vol. 56, pp. 04CE13-1–04CE13-4, Mar. 2017.

[29] K. Kinoshita, "Improving memory performance of Cu/HfO_2/Pt conducting-bridge RAM by solvent substitution," *ECS Trans.*, vol. 69, pp. 11–17, Sep. 2015.

[30] H. Minamimoto, H. Irie, T. Uematsu, T. Tsuda, A. Imanishi, S. Seki, and S. Kuwabata, "Polymerization of room-temperature ionic liquid monomers by electron beam irradiation with the aim of fabricating three-dimensional micropolymer/nanopolymer structures," *Langmuir*, vol. 31, no. 14, pp. 4281–4289, Apr. 2015.

[31] B. D. Ratner, J. J. Rosen, A. S. Hoffman, and L. H. Scharpen, "An ESCA study of surface contaminants on glass substrates for cell adhesion," in *Surface Contamination: Genesis, Detection and Control*, vol. 2, K. L. Mittal, Ed. New York, NY, USA: Plenum, 1979, pp. 669–686.

[32] S. Caporali, C. Chiappe, T. Ghilardi, C. S. Pomelli, and C. Pinzino, "Coordination environment of highly concentrated solutions of Cu^{II} in ionic liquids through a multidisciplinary approach," *Chem. Phys. Chem.*, vol. 13, no. 7, pp. 1885–1892, May 2012.

[33] S. Poulston, P. M. Parlett, P. Stone, and M. Bowker, "Surface oxidation and reduction of CuO and Cu_2O studied using XPS and XAES," *Surf. Interface Anal.*, vol. 24, no. 12, pp. 811–820, Nov. 1996.

[34] S. Caporali, M. Pedio, C. Chiappe, C. S. Pomelli, R. G. Acres, and U. Bardi, "Surface study of metal-containing ionic liquids by means of photoemission and absorption spectroscopies," *Surf. Sci.*, vol. 648, pp. 360–365, Jun. 2016.

[35] Y.-M. Chang, J. Leu, B.-H. Lin, Y.-L. Wang, and Y.-L. Cheng, "Comparison of H_2 and NH_3 treatments for copper interconnects," *Adv. Mater. Sci. Eng.*, vol. 2013, p. 825195, 2013.

[36] Y. Wang, Q. Liu, S. Long, W. Wang, Q. Wang, M. Zhang, S. Zhang, Y. Li, Q. Zuo, J. Yang, and M. Liu, "Investigation of resistive switching in Cu-doped HfO_2 thin film for multilevel non-volatile memory applications," *Nanotechnology*, vol. 21, no. 4, Jan. 2010, Art. no. 045202.

[37] N. Shukla, B. Grisafe, R. K. Ghosh, N. Jao, A. Aziz, J. Frougier, M. Jerry, S. Sonde, S. Rouvimov, T. Orlova, S. Gupta, and S. Datta, "Ag/HfO_2 based threshold switch with extreme non-linearity for unipolar cross-point memory and sweep-slope phase-FETs," in *IEDM Tech. Dig.*, Dec. 2016, pp. 34.6.1–34.6.4.

[38] A. Bricalli, E. Ambrosi, M. Laudato, M. Maestro, R. Rodriguez, and D. Ielmini, "SiO_X-based resistive switching memory (RRAM) for crossbar storage/select elements with high on/off ratio," in *IEDM Tech. Dig.*, Dec. 2016, pp. 4.3.1–4.3.4.

[39] Y. Yang, P. Gao, S. Gaba, T. Chang, X. Pan, and W. Lu, "Observation of conducting filament growth in nanoscale resistive memories," *Nature Commun.*, vol. 3, no. 1, p. 1737, Jan. 2012.

[40] M. Y. Chougale, S. R. Patil, S. P. Shinde, S. S. Khot, A. A. Patil, A. C. Khot, S. S. Chougule, C. K. Volos, S. Kim, and T. D. Dongale, "Memristive switching in ionic liquid–based two-terminal discrete devices," *Ionics*, vol. 25, no. 11, pp. 5575–5583, Nov. 2019.

[41] Q. Sheng, Y. Xie, J. Li, X. Wang, and J. Xue, "Transporting an ionic-liquid/water mixture in a conical nanochannel: A nanofluidic memristor," *Chem. Commun.*, vol. 53, no. 45, pp. 6125–6127, 2017.

[42] K. Rajan, A. Chiappone, D. Perrone, S. Bocchini, I. Roppolo, K. Bejtka, M. Castellino, C. F. Pirri, C. Ricciardi, and A. Chiolerio, "Ionic liquid-enhanced soft resistive switching devices," *RSC Adv.*, vol. 6, no. 96, pp. 94128–94138, 2016.

HIROSHI SATO received the B.E. degree from the Department of Applied Physics, Tokyo University of Science, Tokyo, Japan, in 2019. He is currently pursuing the M.E. degree with the Graduate School of Science, Tokyo University of Science. He has been working as a Research Assistant with the National Institute of Advanced Industrial Science and Technology, since 2018.

HISASHI SHIMA received the B.E., M.E., and Ph.D. degrees from Tohoku University, Sendai, Japan, in 2001, 2003, and 2005, respectively. He is currently a Senior Researcher with the Nanoelectronics Research Institute (NeRI), National Institute of Advanced Industrial Science and Technology (AIST), Japan. His current activities include the development of non-volatile memory and neuromorphic devices utilizing redox reactions.

YUSEI HONMA graduated from the National Institute of Technology, Tsuruoka College, Yamagata, Japan, in 2017. He joined ULVAC Techno Ltd., Japan, where he is currently an Engineer. and specializes in maintenance and development for various types of high-vacuum equipment, such as sputtering and dry-etching systems. From 2018 to 2020, he was an Assignee with the National Institute of Advanced Industrial Science and Technology, Japan, and in charge of the microfabrication processes to prepare IL-CBRAM devices used in this study.

YASUHISA NAITOH received the M.E. and Ph.D. degrees from Osaka University, Osaka, Japan, 2000 and 2003, respectively. From 2002 to 2003, he was a Researcher with Motorola, USA. He is currently a Senior Researcher with the National Institute of Advanced Industrial Science and Technology (AIST), Japan. His current research interest includes electronics devices based on nanostructures.

HIROYUKI AKINAGA (Member, IEEE) received the B.E., M.E., and Ph.D. degrees from the University of Tsukuba, Japan, in 1987, 1989, and 1992, respectively. He is currently the Principal Research Manager with the Device Technology Research Institute, National Institute of Advanced Industrial Science and Technology (AIST), and the Deputy Research Supervisor of the project of Scientific Innovation For Energy Harvesting Technology, Japan Science and Technology Agency (JST). He has been serving as a Convenor with the International Electrotechnical Commission (IEC), TC113 (Nanotechnology for electrotechnical products and systems). His current research interests include nanoelectronics and open innovation platform. He is a fellow of the Japan Society of Applied Physics.

TOSHIKI NOKAMI was born in Wakayama, Japan. He received the Ph.D. degree from Kyoto University, in 2004, under the supervision of Prof. Jun-ichi Yoshida. Then, he spent 11 months in ETH Zurich, as a Postdoctoral Fellow, under the direction of Prof. Peter Seeberger. In 2005, he joined Kyoto University, as an Assistant Professor and promoted to a Lecturer, in 2011. He moved to Tottori University, as an Associate Professor, in 2012, and has been a Professor, since 2019. His research interests include organic electrochemistry, functional ionic liquids, and carbohydrates.

TOSHIYUKI ITOH graduated from the Tokyo University of Education, in 1976, and received the Ph.D. degree from The University of Tokyo, in 1986. He worked as a chemistry teacher in two high schools in his home prefecture of Mie. He was appointed as an Assistant Professor with Okayama University, in 1987, where he was promoted to an Associate Professor, in 1990. He worked with Prof. Dr. Anthony G. M. Barrett with Colorado State University, from1990 to 1991, and moved to Tottori University, in 2002, where he was promoted to a Full Professor, in 2004, and retired, in 2019. After retirement from Tottori University, he served as a Specially Appointed Professor with Tottori University for one year, then moved to the present institute, in April 2020. He is currently a fellow with the Toyota Physical and Chemical Research Institute and an Emeritus Professor with Tottori University. He was elected as a fellow of the Royal Society of Chemistry (FRSC), in 2017. He served as a Program Officer of the Japan Society for the Promotion of Science (JSPS), from 2012 to 2015, the President of the Society of Fluorine Chemistry, Japan, from 2013 to 2015, and a Representative of the Managing Committee of the Ionic Liquids Research Association, Japan, from 2014 to 2017. He was a recipient of the Society of Synthetic Organic Chemistry Japan Award, in 2010, and the 8th Green and Sustainable Chemistry Award, in 2009.

KENTARO KINOSHITA received the Ph.D. degree from The University of Tokyo, Tokyo, Japan, in 2004. He joined Fujitsu Laboratories Ltd., Atsugi, Japan, in 2004, and moved to Tottori University, Tottori, Japan, in 2008. In 2017, he joined the Tokyo University of Science, Tokyo, as an Associate Professor. His research interests include functional devices, memory, and neuromorphic devices.